

Porous Carbon Derived from Sweet Potato Biomass as Electrode for Zinc-ion Hybrid Supercapacitors

Hongyu Hu¹, Guojiang Wu^{2,*}

¹ Hefei No.8 Highschool, 1688 Xiyou Road, Hefei 230071, Anhui, P.R. China.

² Institute of Plasma Physics, Hefei Institutes of Physical Science, Chinese Academy of Sciences, Hefei 230031, People's Republic of China

*E-mail: gjuwu@ipp.ac.cn (G. Wu)

Received: 11 April 2021 / Accepted: 4 June 2021 / Published: 10 August 2021

Zinc-ion hybrid supercapacitors (Zn-HSC) with outstanding capacity, durable longevity and low cost offer an opportunity for the development of electrochemical energy storage devices. Nevertheless, the development of Zn-HSC is still in its initial stage and there are many problems exist. In particular, the difficulty caused by restricted adsorptive capability of carbon cathode significantly limits the energy density of Zn-HSC. Herein, a novel sort of activated carbon (AC) with high surface area of 3424 m² g⁻¹ was obtained from a common biomass through economical method for pyrolysis activation. The Zn-HSC demonstrated a high discharge capacitance (336 F g⁻¹ at 0.5 A g⁻¹), remarkable energy density (112 Wh kg⁻¹ at 385 W kg⁻¹), and 93% capacitance retention after 10000 cycles at 5 A g⁻¹.

Keywords: activated carbon; high surface area; biomass; zinc-ion hybrid supercapacitors

1. INTRODUCTION

With the global commercial and technological development, people are prompted to search for the energy storage devices with lower cost, higher power density and more durable features. For instance, the Lithium-ion battery (LIB) have shown its excellent function for many years [1-2]. Nevertheless, the short battery life and slow charging rate still remain as the problems of this alternatives [3-6]. By contrast, electrochemical capacitors are well known for their fast-charging rate and high-power density in addition to their security [7-9]. The energy density of it, however, is limited [10-12], which lead the scientists to search for alternatives to the conventional supercapacitors. For helping these two energy storage devices compensate for themselves, researchers have been widely investigating the hybrid supercapacitors since a few decades ago [13-15].

Hybrid supercapacitors based on lithium-ion have been extensively investigated for its perfect performance in electrochemical reactions [16-17]. Nonetheless, the shortage of Li resources,

flammability and limited storage bothered researchers for many years, prompting them to discover alternative hybrid supercapacitors based on other monovalent cations such as Na^+ , K^+ , Ca^{2+} and Zn^{2+} [18-23]. Among a large number of different ions, Zn-HSC plays one of the best roles for their distinct characteristics: less air sensitive, more portable, and higher capacity than Li-ion-based supercapacitors [24-26]. Such remarkable achievements inspire increasing researcher's efforts in the discovery of Zn-HSC with excellent behavior. Tian et al reported the first Zn-HSC device that delivered 53 F g^{-1} by fitting a positive electrode of carbon nanotube with negative electrode of Zn in a ZnSO_4/PVA electrolyte [27]. Then, energy storage devices were set out by Wang et al by adopting Zn foil, AC, and $\text{Zn}(\text{CF}_3\text{SO}_3)_2$ in acetonitrile. This device shows better electrochemical behavior, such as a high capacitance of 170 F g^{-1} , and long lifespan up to 20000 cycles with 91% capacitance retention [28]. Besides, another Zn-HSC with an AC cathode reached a discharge capacity of 121 mAh g^{-1} , and 91% capacitance retention after 10,000 cycles [29]. After that, a large number of tactics have been proposed to optimize the electrochemical characteristics of Zn-HSC.

Nevertheless, the development of Zn-HSC is still in its initial stage and there are many problems exist. In particular, the difficulty caused by restricted adsorption capability of carbon cathode significantly limits the energy density of Zn-HSC [30]. The adsorption capability was restricted because of the deficient specific surface areas of carbon cathode and the intrinsically insufficient charge storage capacity via physical absorption/desorption of Zn ions in the Helmholtz layer. Therefore, it's pivotal to design novel carbon cathode with high energy density. Recent studies have pointed out that the porous N-doped carbon is extremely favored with improving Zn ions' the chemical adsorption process between the electrode and electrolyte [31]. In addition, for porous carbon materials, the optimal pore size is between 0.8–2.0 nm(microscope) for the electroadsorption of hydrated ions [32]. The substantial micropores also have the merits for high specific surface area loading more active sites and abundant pore structure for ion transport, which are beneficial to the amelioration of capacitance behavior.

Inspired by these studies, a novel sort of ZnCl_2 templating porous carbon from the biomass of the sweet potato powder with abundant nitrogen element was derived by a simple pyrolysis activation method in this paper. The derived AC has high surface area of $3424 \text{ m}^2 \text{ g}^{-1}$ with substantial micropores and functional groups of N atoms. By employing this cathode, the Zn-HSC demonstrated a high discharge capacitance (336 F g^{-1} at 0.5 A g^{-1}), remarkable energy density (112 Wh kg^{-1} at 385 W kg^{-1}), and long lifespan up to 10000 cycles at 5 A g^{-1} with 93% retention.

2. EXPERIMENTAL PART

2.1 Preparation of ZnCl_2 templating AC:

Sweet potato powders were purchased from Rong-Fang flagship store (China). All other reagents were purchased from Sinopharm Chemical Reagent Co. Ltd. Activated carbon (AC) electrodes were prepared from sweet potato powders. Firstly, weigh and grind 3 g powders of sweet potatoes, 1 g zinc chloride, 1 g sodium chloride with 30 g water until there are some white deposits. Secondly, the sample was dried at $100 \text{ }^\circ\text{C}$ for 1h (gel is formed). Thirdly, the sample was transferred to the quartz tube furnace

at 600 °C for 1 h degrees per minutes until it attains 600 °C, then cooled naturally. Fourthly, the sample was grinded with solid KOH at a weight ratio of 1:3, and after that, the mixture was heated at 600 °C for 2 h. Fifthly, the sample was activated for 1 h at 800 °C. Finally, the products were obtained by the cleaning of using diluted HCl solution and deionized.

2.2 Characterization

The morphology and phase of AC were derived by scanning electron microscopy (SEM, GeminiSEM 500), and X-ray diffraction (XRD, Cu K α , 1.5418 Å), separately. Raman scattering spectra was carried out on a Renishaw System 2000 spectrometer by adopting 514.5 nm Ar⁺ excitation line. The samples' porosities and surface areas were tested by a surface area and porosity analyzer (TriStar II 3020 V1.03). The X-ray photoelectron spectroscopy (XPS) was measured by a Thermo ESCALAB250Xi spectrometer using monochromatized Al K α (h ν = 1486.6 eV) as the excitation source.

2.3 Electrochemical measurements:

Galvanostatic cha-discharging (GCD) was studied separately at 0.5, 1, 2, 5, 10, and 20 A g⁻¹, using an electrochemical station (CHI660e). Cyclic voltammetry (CV) curves were measured separately at 2, 5, 10, 20, 50, and 100 mV s⁻¹, also by adopting CHI660e.

2.4 Zn-HSC preparation

The anode electrode is zinc foil, which is pouched into a 16 mm diameter electrode. The cathode electrode consists 80 wt% of AC, 10 wt% of Polytetrafluoroethylene (PTFE), and 10 wt% of carbon black. The mixture was coated stainless steel net with 12 mm diameters. Finally, the prepared electrodes were dried and assembled. After the drying process (at 80 °C for 10 h), the AC cathode//separator//Zn anode was assembled into Zn-HSC, with another two components: 2M ZnSO₄ electrolyte, and CR2032 shell.

3. RESULTS AND DISCUSSION

Morphologies and micro-structure of AC powders were analyzed in Figure 1. (a,b). The irregular shape and rough surface of the AC particles was observed by analyzing the SEM images of AC. Majority of the particles have their size of about 10~30 μ m. Then, XRD analysis was used for finding the crystal morphology of the sample. Figure 1c shows the shapes of AC. In this figure, at about 23 °C and 42 °C, two different peaks were observed which correspond to (002) and (101) planes of graphitic carbon [33-34], while the much weaker and broader (002) peak, indicating that the damage of consistent structural domains and the random distribution of graphene sheets in the AC were resulted by KOH activation [35]. The Raman spectra of AC is shown in Figure 1d. There are two strong peaks at 1335(D-band,

corresponding to disorder carbon atoms with sp^2 hybridization) and 1590 cm^{-1} (G-band, corresponding to the E_{2g} graphitic pattern for the carbon) [33,36], indicating the imperfect structure of the AC and the stretching vibration of the hybrid carbon particles in the graphited crystallites [37]. By analyzing the strength of the two peaks, it represents that the AC has substantial defects, and the result is consistent with the SEM images and XRD analysis. The strength ratio of G-band to D-band is used to indicate the order of carbon material, while the strength of G-band is higher than that of D-band shows that the as-prepared carbon material is partially graphitized [38].

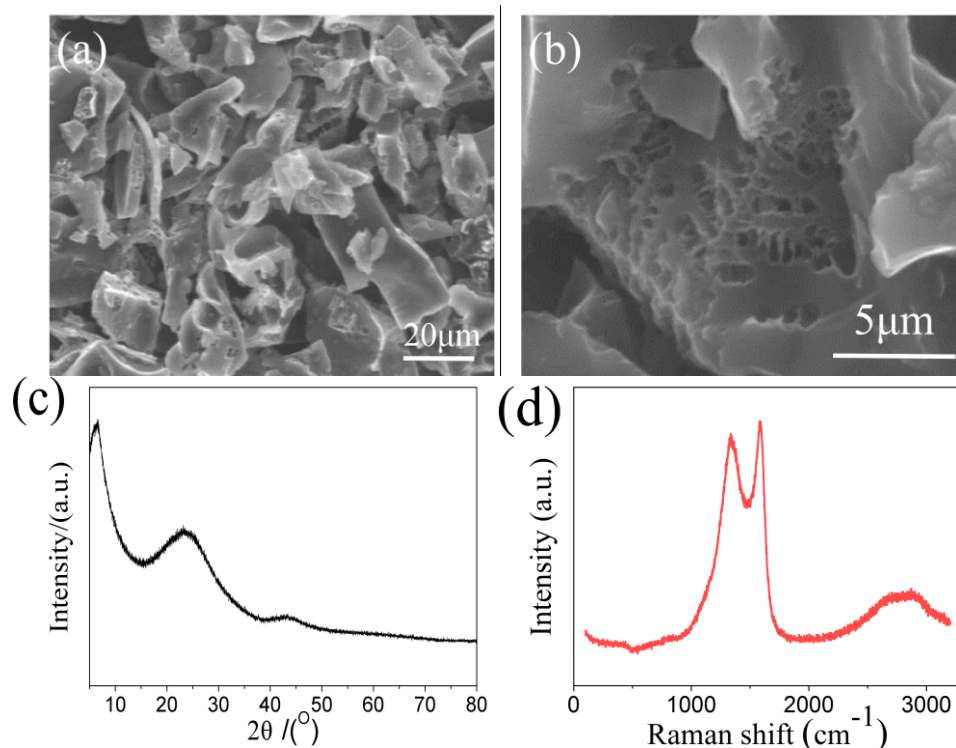


Figure 1. (a,b) SEM images, (c) X-ray pattern, and (d) Raman spectrum of AC.

The porosity of AC was extensively excavated by N_2 absorption/desorption isothermal analysis, shown in Figure 2a. At relative pressure P/P_0 from 0 to 0.3, the absorption of N_2 increases rapidly, indicating the appearance of substantial micropores [39]. A large number of micropores will help improve the double layer capacitance of active materials [33,40]. The pore size distribution further confirms this result. As shown in Figure 2b, it's obvious that the pore size is in the range of 1-3 nm, which offers a high specific surface area of $3424\text{ m}^2\text{g}^{-1}$.

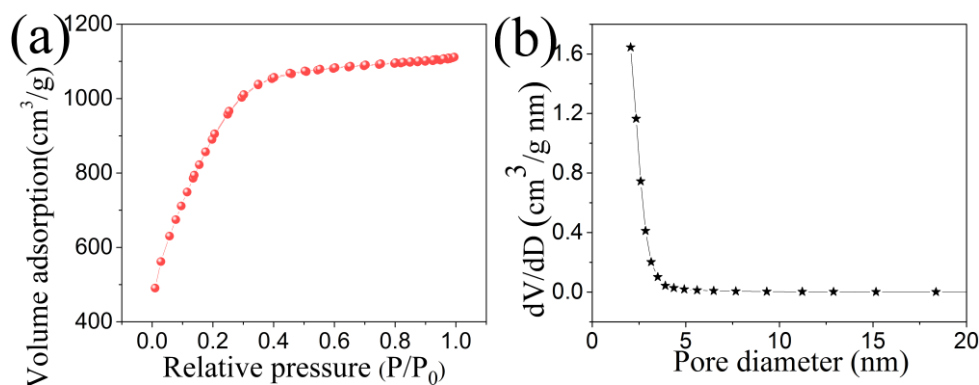


Figure 2. (a) the isotherms of N₂ adsorption-desorption and (b) pore size distribution curve of AC.

In order to gain chemical composition of the AC, XPS was adopted. Only C, N and O elements were detected (Figure 3a). Furthermore, the deconvoluted N 1s spectra includes three peaks, pyrrolic-N (399.9 eV), quaternary-N (401.3 eV), and nitrogen oxides (402.2 eV) (Figure 3b) [33, 41]. The wettability [31] and charge accumulation can be improved [41], when this containing-N AC is used as the cathode electrode. Besides, it is energetically favored with improving the Zn ions' chemical adsorption process at the electrode/electrolyte interface [31].

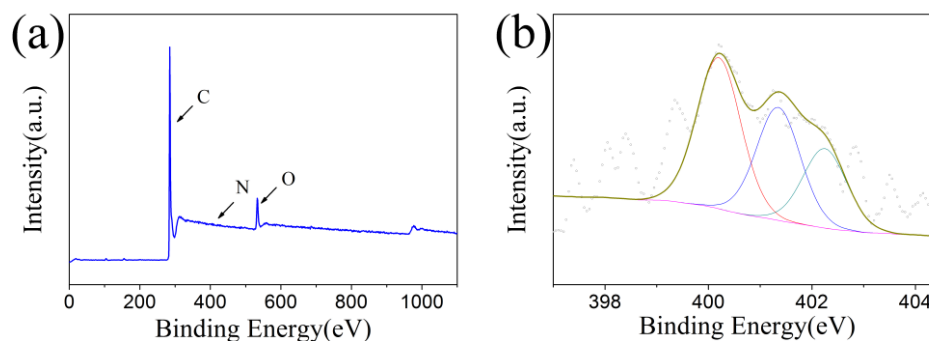


Figure 3. (a) XPS spectra of AC (b) N1s spectra of AC

CV and GCD were implemented to assess electrochemical performance of Zn-HSC. As shown in Figure 4a, from 2 to 100 mV s⁻¹ (the scan rate), the CV curves exhibit an approximately rectangular shape with a slight Faraday peak, which indicates the capacitance and pseudocapacitance network [42]. The N elements in AC may make a contribution to pseudocapacitance, thus increasing the capacitance. More importantly, the N-doping AC can effectively enhance electrical conductivity and wettability of the AC electrode, and then improve the ion transfer efficiency and energy storage capacity [43-44]. The current rises with the scan rate growing, and the CV plots hold similar shapes at various scan rates. This phenomenon indicates its rapid kinetics and effectiveness in storing zinc ion even when the electrochemical reaction process was extremely fast. After analyzing the GCD measurements at various current density (Figure 4b), the specific capacitances were found 336, 312, 260, 215, 158 and 106 F g⁻¹ at 0.5, 1, 2, 5, 10 and 20 A g⁻¹, respectively. Meanwhile, it showed the high energy density of 115 Wh kg⁻¹ (at 385 W kg⁻¹). The charge and discharge cycle stability is pivotal in deciding the total function of

Zn-HSC. To test the durability of Zn-HSC, GCD was taken at 5 A g^{-1} for 10,000 cycles, as shown in Figure 4c. We found that the capacitance retention is almost 93%, where the remarkable electrochemical stability is shown clearly. Performance comparison of various biomass based AC cathodes for Zn-HSC were shown in Table 1. The performance of our materials is better than most of the reported biomass materials, and sweet potato is rich in resources and low cost, which is a potential material choice for Zn-HSC.

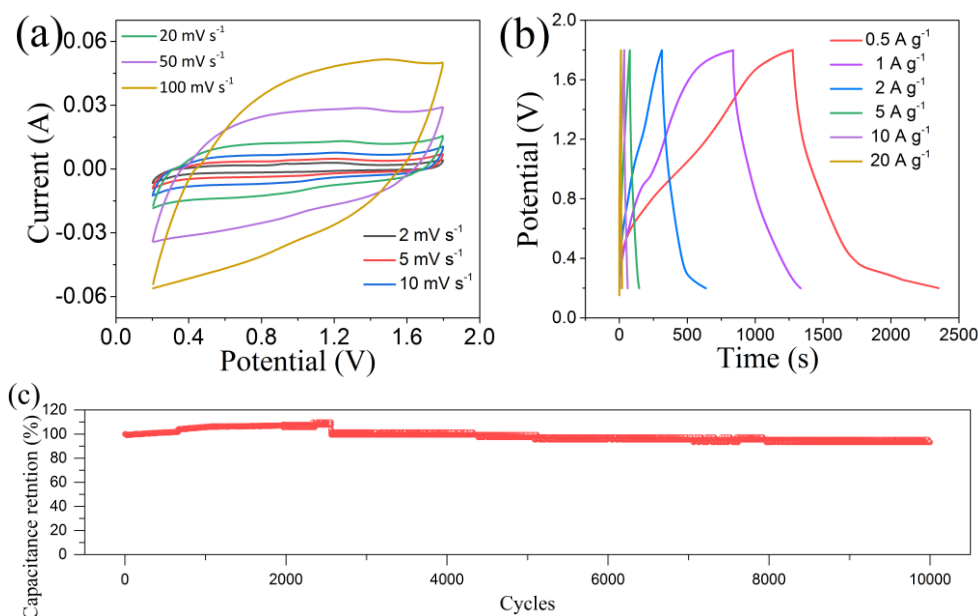


Figure 4. (a) CV plots of Zn-HSC at various sweep rates. (b) GCD plots of Zn-HSC at different current densities. (c) Cycling stability of Zn-HSC at 5 A g^{-1} .

Table 1. Performance comparison of various biomass based AC cathodes for Zn-HSC

Cathode materials	SBET ($\text{m}^2 \text{ g}^{-1}$)	Specific capacity ($\text{Wh kg}^{-1} / \text{W kg}^{-1}$)	Cycling stability / Retention (cycles / A g^{-1} / %)	Ref.
kelp blades	3047	111.5 / 1300	100 / \ / 95	[45]
bone glue	3657.5	168 / 327	10000 / 5 / \	[46]
bagasse and coconut shell	3401	118 / \	20000 / 2 / 94.9	[47]
wood	1248	109.5 / 225	50000 / 2 / 92.7	[41]
coconut shells	3384	52.7 / 1725	20000 / 2 / 91	[24]
Sweet potato powders	3424	115 / 385	10000 / 5 / 93	This work

Figure 5 (a,b) suggests that the SEM images of Zn anode before and after 10,000 times tests. At its initial condition, the surface of the Zn anode is significantly glossy with bright metal luster. However, after 10,000 tests, the Zn anode are covered with small grains and alight cracks with some impurities, and Zn anode also changes to dark gray color, losing its metal luster. This phenomenon is similar to that reported by Zhao et al [26]. This phenomenon is possibly resulting from the change of surface structure on the Zn anode. Compared XRD images of the Zn anode before and after cycling in Figure 5c, we found that the $\text{Zn}_4\text{SO}_4(\text{OH})_6 \cdot 5\text{H}_2\text{O}$ (PDF#39-0688) was produced [23], which may be the reason why the performance of Zn-HSC becomes lower.

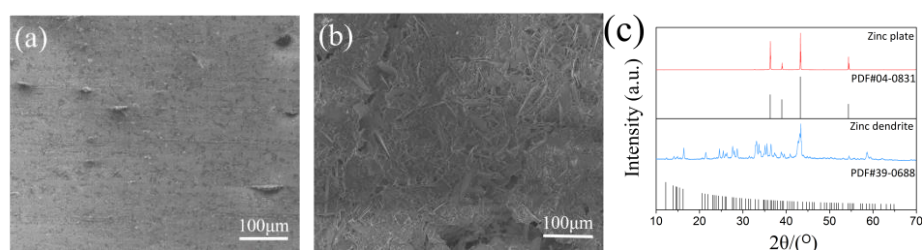


Figure 5. (a) SEM image of zinc foils before 10,000 cycling. (b) SEM image of zinc foils after 10,000 cycling (c) XRD patterns of zinc foils before and after 10,000 cycling.

4. CONCLUSIONS

To conclude, we successfully developed a new Zn-HSC via directly projecting Zn foil as anode electrode and bio-carbon as the cathode electrode. The Zn-HSC showed outstanding electrochemical behavior. It shows high performance in the range of 0.2–1.8 V, offering a remarkable capacitance of 336 F g^{-1} (0.5 A g^{-1}). The Zn-HSC showed specific capacities of 312, 260, 215, 158 and 106 F g^{-1} at 1, 2, 5, 10 and 20 A g^{-1} , respectively. In the meantime, it showed the excellent energy density of 112 Wh kg^{-1} (at 385 W kg^{-1}). In addition, our Zn-HSC also showed excellent cycling stability (93% capacity retention after 10,000 cycles at 5 A g^{-1}). This study will help to ameliorate the future of energy storage devices.

ACKNOWLEDGEMENT

The study was supported by Key Laboratory of Photovoltaic and Energy Conservation Materials, Chinese Academy of Sciences, Hefei 230031, People's Republic of China.

References

1. B. Liu, Y. Sun, L. Liu, J. Chen, B. Yang, S. Xu, X. Yan, *Energ. Environ. Sci.*, 12 (2019) 887-922.
2. B. Dunn, H. Kamath, J.-M. Tarascon, *Science*, 334 (2011) 928-935.
3. M.N. Obrovac, V.L. Chevrier, *Chem. Rev.*, 114 (2014) 11444-11502.
4. S. Zheng, Z.-S. Wu, S. Wang, H. Xiao, F. Zhou, C. Sun, X. Bao, H.-M. Cheng, *Energy Storage*

- Mater.*, 6 (2017) 70-97.
5. A.X. Wang, X.F. Hu, H.Q. Tang, C.Y. Zhang, S. Liu, Y. W. Yang, Q.H. Yang, J.Y. Luo, *Angew. Chem. Int. Ed.*, 56 (2017) 11921-11926.
 6. Q. Zeng, Y. Li, K.-H. Wu, N. Huang, S. Dalapati, B.-J. Su, L.-Y. Jang, I.R. Gentle, D. Jiang, D.-W. Wang, *Energy Storage Mater.*, 12 (2018) 30-36.
 7. P. Simon, Y. Gogotsi, *Nat. Mater.*, 7 (2008) 845-854.
 8. Y. Cho, S. Pak, Y.-G. Lee, J.S. Hwang, P. Giraud, G.-H. An, S. Cha, *Adv. Funct. Mater.*, 30 (2020).
 9. G.-H. An, D.-Y. Lee, H.-J. Ahn, *J. Mater. Chem. A*, 5 (2017) 19714-19720.
 10. L. Liu, L. Su, J. Lang, B. Hu, S. Xu, X. Yan, *J. Mater. Chem. A*, 5 (2017) 5523-5531.
 11. Y. Li, Z. Li, P.K. Shen, *Adv. Mater.*, 25 (2013) 2474-2480.
 12. J. Liu, L. Zhang, H.B. Wu, J. Lin, Z. Shen, X.W. Lou, *Energ. Environ. Sci.*, 7 (2014) 3709-3719.
 13. X. Zheng, H. Wang, C. Wang, Z. Deng, L. Chen, Y. Li, T. Hasan, B.-L. Su, *Nano Energy*, 22 (2016) 269-277.
 14. B. Zhao, D. Chen, X. Xiong, B. Song, R. Hu, Q. Zhang, B.H. Rainwater, G.H. Waller, D. Zhen, Y. Ding, Y. Chen, C. Qu, D. Dang, C.-P. Wong, M. Liu, *Energy Storage Mater.*, 7 (2017) 32-39.
 15. J. Ding, W. Hu, E. Paek, D. Mitlin, *Chem. Rev.*, 118 (2018) 6457-6498.
 16. G. Li, Z. Yang, Z. Yin, H. Guo, Z. Wang, G. Yan, Y. Liu, L. Li, J. Wang, *J. Mater. Chem. A*, 7 (2019) 15541-15563.
 17. H. Li, J. Lang, S. Lei, J. Chen, K. Wang, L. Liu, T. Zhang, W. Liu, X. Yan, *Adv. Funct. Mater.*, 28 (2018) 1800757.
 18. X. Wang, L. Liu, Z. Niu, *Mater. Chem. Front.*, 3 (2019) 1265-1279.
 19. Y. Li, H. Wang, L. Wang, Z. Mao, R. Wang, B. He, Y. Gong, X. Hu, *Small*, 15 (2019) 1804539.
 20. Z. Zhang, M. Li, Y. Gao, Z. Wei, M. Zhang, C. Wang, Y. Zeng, B. Zou, G. Chen, F. Du, *Adv. Funct. Mater.*, 28 (2018) 1802684.
 21. L. Fan, K. Lin, J. Wang, R. Ma, B. Lu, *Adv. Mater.*, 30 (2018) 1800804.
 22. N.Z. Wu, W.J. Yao, X.H. Song, G. Zhang, B.J. Chen, J.H. Yang, Y.B. Tang, *Adv. Energy Mater.*, 9 (2019) 1803865.
 23. L. Dong, X. Ma, Y. Li, L. Zhao, W. Liu, J. Cheng, C. Xu, B. Li, Q.-H. Yang, F. Kang, *Energy Storage Mater.*, 13 (2018) 96-102.
 24. H. Wang, M. Wang, Y. Tang, *Energy Storage Mater.*, 13 (2018) 1-7.
 25. G.-H. An, *Appl. Surf. Sci.*, 530 (2020) 147220.
 26. P. Zhao, B. Yang, J. Chen, J. Lang, T. Zhang, X. Yan, *Acta Phys.-Chim. Sin.*, 36 (2020) 1904050.
 27. Y. Tian, R. Amal, D.-W. Wang, *Front. Energy Res.*, 4 (2016) 00034.
 28. Q. Yang, G.J. Bang, Y. Guo, Z.X. Liu, B.X. Yon, D.H. Wang, Z.D. Huang, X.L. Li, J. Fan, C.Y. Zhi, *Adv. Mater.*, 31 (2019) 1903778.
 29. X. Ma, J. Cheng, L. Dong, W. Liu, J. Mou, L. Zhao, J. Wang, D. Ren, J. Wu, C. Xu, F. Kang, *Energy Storage Mater.*, 20 (2019) 335-342.
 30. L. Dong, W. Yang, W. Yang, Y. Li, W. Wu, G. Wang, *J. Mater. Chem. A*, 7 (2019) 13810-13832.
 31. H. Zhang, Q. Liu, Y. Fang, C. Teng, X. Liu, P. Fang, Y. Tong, X. Lu, *Adv. Mater.*, 31 (2019) 1904948.
 32. C. Lin, J.A. Ritter, B.N. Popov, R.E. White, *J. Electrochem. Soc.*, 146 (1999) 3168-3175.
 33. S. Yang, S.L. Wang, X. Liu, L. Li, *Carbon*, 147 (2019) 540-549.
 34. Y.Q. Zhang, X. Liu, S.L. Wang, S.X. Dou, L. Li, *J. Mater. Chem. A*, 4 (2016) 10869-10877.
 35. B. Liu, H. Chen, Y. Gao, H. Li, *Electrochim. Acta*, 189 (2016) 93-100.
 36. W. Fan, Y.Y. Xia, W.W. Tjiu, P.K. Pallathadka, C.B. He, T.X. Liu, *J. Power Sources*, 243 (2013) 973-981.
 37. H.W. Wang, H. Yi, C.R. Zhu, X.F. Wang, H.J. Fan, *Nano Energy*, 13 (2015) 658-669.
 38. G.P. Hao, A.H. Lu, W. Dong, Z.Y. Jin, X.Q. Zhang, J.T. Zhang, W.C. Li, *Adv. Energy Mater.*, 3 (2013) 1421-1427.
 39. P. Ramakrishnan, S. Shanmugam, *J. Power Sources*, 316 (2016) 60-71.

40. D.W. Wang, F. Li, M. Liu, G.Q. Lu, H.M. Cheng, *Angew. Chem. Int. Ed.*, 47 (2008) 373-376.
41. G.B. Lou, G. Pei, Y.T. Wu, Y.Z. Lu, Y.T. Wu, X.Q. Zhu, Y.J. Pang, Z.H. Shen, Q. Wu, S.Y. Fu, H. Chen, *Chem. Eng. J.*, 413 (2021) 127502.
42. Y.M. Wang, T. Liu, X.J. Lin, H. Chen, S. Chen, Z.J. Jiang, Y. Chen, J. Liu, J.L. Huang, M.L. Liu, *ACS Sustain. Chem. Eng.*, 6 (2018) 13932-13939.
43. L.F. Chen, X.D. Zhang, H.W. Liang, M.G. Kong, Q.F. Guan, P. Chen, Z.Y. Wu, S.H. Yu, *ACS Nano*, 6 (2012) 7092-7102.
44. X.Q. Yang, D.C. Wu, X.M. Chen, R.W. Fu, *J. Phys. Chem. C*, 114 (2010) 8581-8586.
45. J. Zeng, L.B. Dong, L.L. Sun, W. Wang, Y.H. Zhou, L. Wei, X. Guo, *Nano-Micro Lett.*, 13 (2021) 19.
46. W.J. Fan, J. Ding, J.N. Ding, Y.L. Zheng, W.Q. Song, J.F. Lin, C.X. Xiao, C. Zhong, H.L. Wang, W.B. Hu, *Nano-Micro Lett.*, 13 (2021) 59.
47. P.F. Yu, Y. Zeng, Y.X. Zeng, H.W. Dong, H. Hu, Y.L. Liu, M.T. Zheng, Y. Xiao, X.H. Lu, Y.R. Liang, *Electrochim. Acta*, 327 (2019) 134999.

© 2021 The Authors. Published by ESG (www.electrochemsci.org). This article is an open access article distributed under the terms and conditions of the Creative Commons Attribution license (<http://creativecommons.org/licenses/by/4.0/>).